JOURNAL OF COMPUTATIONAL PHYSICS 76, 243–262 (1988)

Optimal Choice of Grid Points in Multidimensional Pseudospectral Fourier Methods

R. H. BISSELING* AND R. KOSLOFF

Department of Physical Chemistry and the Fritz Haber Molecular Dynamics Research Center, The Hebrew University, Jerusalem, 91904 Israel

Received February 13, 1987; revised June 17, 1987

The optimal choice of grid points for the multi-dimensional pseudospectral Fourier method is investigated. Optimal sampling is obtained by looking for the most isotropic sampling grid in momentum space. The points of this grid are found to be positioned at the center of densely packed hard spheres forming an oblique grid. It is found that by using this oblique grid the sampling efficiency can be enhanced, compared to a rectangular grid, by a factor ranging from 1.4 for three dimensions to 16 for eight dimensions. The method is checked in five dimensions by calculating the Laplacian in an oblique and in a Cartesian grid. The oblique grid was found to have superior accuracy using a factor of 2.5 less grid points. The method is also illustrated in six dimensions by a calculation of the ground and first excited states of two interacting triplet hydrogen atoms

I. Introduction

Partial differential equations are of great importance in physics. Almost all the fundamental laws are formulated in terms of partial differential equations. Among the equations which are frequently encountered are the equation of Maxwell, of electromagnetics, the Helmholtz classical wave equation, the diffusion equation, the Schrödinger equation of quantum mechanics and more. Therefore it is not surprising that large efforts have been devoted to the development of numerical methods for solving partial differential equations. This paper is motivated particularly toward the solution of the time dependent Schrödinger equation

$$i\frac{\partial\psi}{\partial t}=\hat{\mathbf{H}}\psi, \tag{1.1}$$

where the Hamiltonian operator $\hat{\mathbf{H}}$ is given by

$$\hat{\mathbf{H}}=\frac{-1}{2m}\nabla_n^2+\hat{\mathbf{V}}(r_1, r_2, r_3, ..., r_n),$$

where ∇_n^2 is the n-dimensional Laplacian operator, $\hat{\mathbf{V}}$ is the potential operator, and n is the dimensionality of the system.

* Present address: Koninklijke/Shell-Laboratorium, Amsterdam, P.O. Box 3003, 1003 AA Amsterdam, the Netherlands.

0021-9991/88 $3.00

In recent years pseudospectral methods have gained considerable popularity in the numerical solution of partial differential equations [1]. Pseudospectral or collocation methods approximate the solution u of a partial differential equation by a truncated series

$$u_N(\mathbf{x}) = \sum_{k=0}^{N-1} a_k \phi_k(\mathbf{x}) \tag{1.2}$$

in known functions ϕ_k. The expansion coefficients are chosen so that the approximate solution u_N coincides with the solution u at a discrete set $\mathbf{x}_0, \mathbf{x}_1, ..., \mathbf{x}_{N-1}$ of sampling points

$$u_N(\mathbf{x}_j) = u(\mathbf{x}_j), \qquad j = 0, ..., N-1. \tag{1.3}$$

The solution at other points is obtained by interpolation. The optimal choice of these sampling points is the subject of this work.

The most frequently used pseudospectral method is the Fourier pseudospectral method, or the Fourier method, defined in 1D by equidistant sampling points

$$x_j = j/N, \qquad j = 0, ..., N-1 \tag{1.4}$$

and trigonometric expansion functions

$$\phi_k(x) = e^{2\pi i x k}, \qquad k = 0, ..., N-1. \tag{1.5}$$

In more than one dimension the problem of choosing sampling points becomes more complicated. What is required is an isotropic sampling in momentum space such that the wave motion is represented equally well in all directions. Unfortunately, such isotropic sampling of momentum is impossible in multi-dimensions. The simplest choice of sampling points is on an equidistant rectangular grid. This rectangular grid combined with the multi-dimensional Fourier method is far from optimal; it favours diagonal directions, and as a result samples the directions along the grid axes relatively poorly. Better configurations of sampling points exist; they can be obtained by appropriately skewing the grid. This skewing procedure is the basis for the *skewed Fourier method*, the Fourier method for wave propagation on an oblique grid. Using this oblique grid the sampling efficiency is greatly enhanced compared with the simple rectangular grid. It is found that this enhancement increases with the dimensionality from a factor of 1.4 in 3D to 16 in 8D.

The problem of finding the best skewed grid is related to the dense sphere-packing problem [2–5]. This was first observed by Petersen and Middleton [6], who showed that multi-dimensional interpolation of a class of isotropically band-limited functions is most efficient on an appropriately skewed grid.

For wave packet propagations the maximum represented momentum is limited, and there is no *a priori* knowledge of the direction of the momentum of the wave packet at some stage of the propagation. This means that the momentum vectors are evenly distributed in a sphere of radius $p_{\max}$. The corresponding frequency vectors $\mathbf{k} = \mathbf{p}/2\pi$ lie in a sphere of radius $R = p_{\max}/2\pi$, which is called the *band-limit*

radius of the wave propagation. The band-limit radius is the multi-dimensional analog of the Nyquist frequency.

Sampling a function $f(\mathbf{x})$ on a lattice, i.e., representing it only at discrete lattice points, replaces its Fourier transform $\hat{f}(\mathbf{k})$ by an infinite sum of shifted copies of $\hat{f}(\mathbf{k})$ [7, pp. 189–194]. Each spectrum replica is centered at a point of a lattice that is defined by the reciprocal lattice vectors of the sampling lattice vectors in the $\mathbf{x}$-domain. For wave propagations with band-limit radius R, the spectrum replicas are contained in spheres of radius R with centers at the reciprocal lattice points. As a result the most efficient sampling scheme in the $\mathbf{x}$-domain amounts to densely packing these spheres in a lattice in the $\mathbf{k}$-domain, without overlapping of spheres [6].

The theory of sphere packing [2–5] thus has relevance for the problem of efficient sampling. The densest possible *lattice* packing of spheres is known [2] for dimension at least up to $n = 8$. These lattice packings have been translated into efficient sampling grids by Petersen and Middleton [6].

The skewed Fourier method exploits the above idea of efficient sampling by an oblique grid for propagation of a wave function in time, as opposed to the work of Petersen and Middleton who proposed grid skewing to improve interpolation efficiency.

Use of the skewed Fourier method will cause large savings in computational resources for problems of dimensionality $n \gtrsim 3$. The applications of the Fourier method can be divided into two groups: simulations in real space where the maximum dimensionality is three and simulations in configuration space where the dimensionality is unlimited. An example of the latter is the modeling of processes in molecular dynamics by solving the time dependent Schrödinger equation [8–9]: the dimensionality of the problem is $n = 3L - 3$, where L is the number of atoms participating in the reaction. The motivation for this work is to find means of directly simulating basic chemical reactions such as $A + BC \rightarrow AB + C$ or $AB + CD \rightarrow AC + BD$. Currently most modeling calculations are carried out in two dimensions, the main limitation being the speed and storage capacity of existing computers. The availability of supercomputers has made 3D simulations feasible. The incorporation of parallel architecture into computers will make computations in more than three dimensions feasible in the near future. Projecting on the increase in computation capability it seems possible that full reactive scattering calculations in Cartesian coordinates will be performed in a few years, so that the skewed Fourier method will have much practical applicability.

Section II presents the mathematics of oblique coordinate systems. Section III shows how to sample a function efficiently, on the basis of a dense sphere packing. Section IV summarizes the algorithm of the skewed Fourier method. Section V tests the critical part of the algorithm, the computation of the Laplacian, for a five-dimensional Gaussian wave function. Section VI illustrates the method, applying it to a six-dimensional calculation of the ground and first excited state of two interacting triplet hydrogen atoms in a box. Section VII is the discussion of the results.

II. Transformation to an Oblique Coordinate System

The Laplacian

Let $(\mathbf{e}_1, ..., \mathbf{e}_n)$ be the canonical basis of R^n, and $(\mathbf{v}_1, ..., \mathbf{v}_n)$ a new, not necessarily orthogonal basis. The basis $(\mathbf{v}_1, ..., \mathbf{v}_n)$ will be called the *oblique basis of the* $\mathbf{x}$*-domain.* Let V be the transition matrix from the old to the new basis, i.e., V is the $n \times n$ matrix whose columns are the vectors $\mathbf{v}_j$,

$$V = (v_{ij}) = \begin{pmatrix} v_{11} & v_{12} & \cdots & v_{1n} \\ v_{21} & v_{22} & \cdots & v_{2n} \\ \cdot & \cdot & \cdots & \cdot \\ \cdot & \cdot & \cdots & \cdot \\ v_{n1} & v_{n2} & \cdots & v_{nn} \end{pmatrix} = (\mathbf{v}_1 \cdots \mathbf{v}_n). \tag{2.1}$$

Vectors are written as columns in this paper. The symbol "T" denotes "transposed." Define

$$A = (a_{ij}) = V^{-1}. \tag{2.2}$$

The coordinate representation $\boldsymbol{\lambda} = (\lambda_1, ..., \lambda_n)^T$ of a vector $\mathbf{x} = (x_1, ..., x_n)^T \in R^n$ in the oblique basis of the $\mathbf{x}$-domain is given by

$$\mathbf{x} = \sum_{j=1}^{n} \lambda_j \mathbf{v}_j. \tag{2.3}$$

The relation between $\mathbf{x}$ and $\boldsymbol{\lambda}$ is given by

$$\mathbf{x} = V\boldsymbol{\lambda}, \qquad \boldsymbol{\lambda} = A\mathbf{x}. \tag{2.4}$$

Let $f(\mathbf{x})$ be a complex-valued function on R^n. The function f can be expressed as a function f_1 of the new coordinates, by

$$f_1(\boldsymbol{\lambda}) = f(\mathbf{x}), \tag{2.5}$$

where the function f_1 is defined as

$$f_1 = f \circ V. \tag{2.6}$$

The relation between the derivatives of f and f_1, as obtained by the chain rule, is

$$\frac{\partial f}{\partial x_i}(\mathbf{x}) = \sum_{j=1}^{n} a_{ji} \frac{\partial f_1}{\partial \lambda_j}(\boldsymbol{\lambda}). \tag{2.7}$$

A subsequent application of the chain rule gives the relation between the second derivatives:

$$\frac{\partial^2 f}{\partial x_i^2}(\mathbf{x}) = \sum_{k=1}^{n} \sum_{j=1}^{n} a_{ji} a_{ki} \frac{\partial^2 f_1}{\partial \lambda_k \, \partial \lambda_j}(\boldsymbol{\lambda}). \tag{2.8}$$

The Laplacian of f can be expressed as a sum of second derivatives of f_1, by

$$\nabla^2 f(\mathbf{x}) = \sum_{i=1}^{n} \frac{\partial^2 f}{\partial x_i^2}(\mathbf{x}) = \sum_{k=1}^{n} \sum_{j=1}^{n} \left(\sum_{i=1}^{n} a_{ji} a_{ki} \right) \frac{\partial^2 f_1}{\partial \lambda_k \, \partial \lambda_j}(\boldsymbol{\lambda})$$
$$= \sum_{k=1}^{n} \sum_{j=1}^{n} b_{jk} \frac{\partial^2 f_1}{\partial \lambda_k \, \partial \lambda_j}(\boldsymbol{\lambda}), \tag{2.9}$$

where the coefficients b_{jk} are defined by

$$b_{jk} = \sum_{i=1}^{n} a_{ji} a_{ki}. \tag{2.10}$$

This is equivalent to

$$B = (b_{jk}) = AA^{\mathrm{T}}. \tag{2.11}$$

Since B is a symmetric matrix, and f is assumed to be many times differentiable, so that $\partial^2 f_1 / \partial \lambda_k \, \partial \lambda_j = \partial^2 f_1 / \partial \lambda_j \, \partial \lambda_k$ for all j, k, the number of terms in Eq. (2.9) can be reduced to about half by symmetrization. This is done by introducing the coefficients c_{jk} of an upper triangular matrix $C = (c_{jk})$, with

$$c_{jk} = \begin{cases} 2b_{jk} & \text{if } j < k \\ b_{kk} & \text{if } j = k \\ 0 & \text{if } j > k. \end{cases} \tag{2.12}$$

As a result, the Laplacian can be written as

$$\nabla^2 f(\mathbf{x}) = (\nabla^2 f)_1(\boldsymbol{\lambda}) = \sum_{k=1}^{n} \sum_{j=1}^{k} c_{jk} \frac{\partial^2 f_1}{\partial \lambda_k \, \partial \lambda_j}(\boldsymbol{\lambda}), \tag{2.13}$$

where the same notation $(\nabla^2 f)_1 = (\nabla^2 f) \circ V$ as in Eq. (2.6) has been used.

The Fourier Transform

The *n-dimensional Fourier transform* of a function $f: R^n \to C$ is defined as [7]

$$\hat{f}(\mathbf{k}) = \int_{R^n} f(\mathbf{x}) \, e^{-2\pi i \mathbf{k} \cdot \mathbf{x}} \, d\mathbf{x}. \tag{2.14}$$

The *inverse Fourier transform* is then given by

$$f(\mathbf{x}) = \int_{R^n} \hat{f}(\mathbf{k}) \, e^{+2\pi i \mathbf{k} \cdot \mathbf{x}} \, d\mathbf{k}. \tag{2.15}$$

Let $(\mathbf{u}_1, \ldots, \mathbf{u}_n)$ be a new basis of R^n, uniquely related to the basis $(\mathbf{v}_1, \ldots, \mathbf{v}_n)$ by

$$(\mathbf{u}_1, \ldots, \mathbf{u}_n) = U = (V^{-1})^{\mathrm{T}}. \tag{2.16}$$

The basis $(\mathbf{u}_1, ..., \mathbf{u}_n)$ will be called the *oblique basis of the* **k***-domain.* The coordinate representation $\boldsymbol{\mu} = (\mu_1, ..., \mu_n)^T$ of a vector $\mathbf{k} = (k_1, ..., k_n)^T \in R^n$ in the oblique basis of the **k**-domain is given by

$$\mathbf{k} = \sum_{j=1}^{n} \mu_j \mathbf{u}_j. \tag{2.17}$$

The relation between **k** and $\boldsymbol{\mu}$ is given by

$$\mathbf{k} = U\boldsymbol{\mu}, \qquad \boldsymbol{\mu} = V^T\mathbf{k}. \tag{2.18}$$

The importance of this particular new basis of the **k**-domain lies in the fact that the Fourier transform is preserved, up to a constant, in the transformation to new bases of the **x**-domain and **k**-domain:

LEMMA 1. *Let* $d = |\det U|$, $\boldsymbol{\mu} \in R^n$, *and* $\mathbf{k} = U\boldsymbol{\mu}$. *Then* $\hat{f}_1(\boldsymbol{\mu}) = d \cdot \hat{f}(\mathbf{k})$.

Proof. By definition

$$\hat{f}_1(\boldsymbol{\mu}) = \int_{R^n} f_1(\boldsymbol{\lambda})\, e^{-2\pi i \boldsymbol{\lambda} \cdot \boldsymbol{\mu}}\, d\boldsymbol{\lambda}. \tag{2.19}$$

Substitute $\boldsymbol{\lambda} = A\mathbf{x}$, with Jacobian $J = |\det(\partial\boldsymbol{\lambda}/\partial\mathbf{x})| = |\det A| = |\det U| = d$, giving

$$\hat{f}_1(\boldsymbol{\mu}) = d \cdot \int_{R^n} f(\mathbf{x})\, e^{-2\pi i (A\mathbf{x}) \cdot (V^T\mathbf{k})}\, d\mathbf{x}. \tag{2.20}$$

The proof is completed if it can be shown that

$$(A\mathbf{x}) \cdot (V^T\mathbf{k}) = \mathbf{x} \cdot \mathbf{k}, \qquad \text{all} \quad \mathbf{x}, \mathbf{k} \in R^n, \tag{2.21}$$

which can also be expressed as

$$\boldsymbol{\lambda} \cdot \boldsymbol{\mu} = (V\boldsymbol{\lambda}) \cdot (U\boldsymbol{\mu}), \qquad \text{all} \quad \boldsymbol{\lambda}, \boldsymbol{\mu} \in R^n. \tag{2.22}$$

It is sufficient to prove that this is true for all basis vectors,

$$(V\mathbf{e}_i) \cdot (U\mathbf{e}_j) = \mathbf{e}_i \cdot \mathbf{e}_j, \qquad \text{all } i, j, \tag{2.23}$$

i.e.,

$$\mathbf{v}_i \cdot \mathbf{u}_j = \delta_{ij}, \qquad \text{all } i, j \tag{2.24}$$

(δ_{ij} is the Kronecker symbol). However, this is equivalent to the matrix equation

$$V^T U = I, \tag{2.25}$$

which is true per definition; see Eq. (2.16). Q.E.D.

The Fourier Transform of the Laplacian

The derivative property of the Fourier transform is [7, Chap. 6]

$$\widehat{\frac{\partial f}{\partial x_j}}(\mathbf{k}) = 2\pi i k_j \hat{f}(\mathbf{k}), \qquad \text{all } \mathbf{k} \in R^n, \tag{2.26}$$

for $j = 1, ..., n$. The Fourier transform of the Laplacian of f in the canonical coordinates is thus given by

$$\widehat{\nabla^2 f(\mathbf{k})} = -4\pi^2 \left(\sum_{j=1}^{n} k_j^2 \right) \hat{f}(\mathbf{k}), \qquad \text{all } \mathbf{k} \in R^n. \tag{2.27}$$

In oblique coordinates the Fourier transform of the original Laplacian is

$$\begin{aligned} \widehat{(\nabla^2 f)_1}(\boldsymbol{\mu}) &= \sum_{k=1}^{n} \sum_{j=1}^{k} c_{jk} \widehat{\frac{\partial^2 f_1}{\partial \lambda_k \, \partial \lambda_j}}(\boldsymbol{\mu}), \qquad \text{(using Eq. (2.13))} \\ &= \sum_{k=1}^{n} \sum_{j=1}^{k} c_{jk}(-4\pi^2 \mu_j \mu_k) \hat{f}_1(\boldsymbol{\mu}), \end{aligned} \tag{2.28}$$

(by application of Eq. (2.26) in the $\boldsymbol{\mu}$-domain), so that

$$\widehat{(\nabla^2 f)_1}(\boldsymbol{\mu}) = L(\boldsymbol{\mu}) \cdot \hat{f}_1(\boldsymbol{\mu}), \tag{2.29}$$

where the quadratic form L is defined by

$$L(\boldsymbol{\mu}) = -4\pi^2 \sum_{k=1}^{n} \sum_{j=1}^{k} c_{jk} \mu_j \mu_k. \tag{2.30}$$

In conclusion, the Laplacian of f can be obtained by the following series of function transformations:

(1)	$f_1 = f \circ V$	(express in oblique coordinates)
(2)	$f_2 = \hat{f}_1$	(Fourier transform)
(3)	$f_3 = L \cdot f_2$	(multiply by L)
(4)	$f_4 = \check{f}_3$	(Fourier transform backwards)
(5)	$\nabla^2 f = f_4 \circ V^{-1}$	(express in canonical coordinates).

III. Efficient Sampling of Band-Limited Functions by Dense Sphere-Packing

Suppose the function f is represented by its values on an infinite discrete grid of points $\mathbf{x} = \sum_{j=1}^{n} \lambda_j \mathbf{v}_j$, where the λ_j are integers. These points form the *lattice* defined by the vectors $\mathbf{v}_1, ..., \mathbf{v}_n$. Since $f_1(\boldsymbol{\lambda}) = f(\mathbf{x})$, this implies that the function f_1 is

represented on the integer grid Z^n, which is rectangular and equidistant, so that the results of sampling theory [7] hold.

In sampling theory it is convenient to analyze the process of sampling using the *Shah* function $\mathrm{III}(\lambda)$ [7, Chap. 5], which is the impulse lattice

$$\mathrm{III}(\lambda) = \sum_{l \in Z^n} \delta(\lambda - l), \tag{3.1}$$

where δ is the Dirac delta function. The sampled function can be defined as

$$g_1(\lambda) = f_1(\lambda) \cdot \mathrm{III}(\lambda). \tag{3.2}$$

Taking Fourier transforms of both sides, and applying the convolution theorem gives

$$\hat{g}_1(\mu) = \hat{f}_1(\mu) * \mathrm{III}(\mu) = \sum_{l \in Z^n} \hat{f}_1(\mu - l), \tag{3.3}$$

where use has been made of the fact that the Shah function is its own Fourier transform [7, Chap. 10]. Note that the function $\hat{g}_1$ is periodic: $\hat{g}_1(\mu + \mathbf{m}) = \hat{g}_1(\mu)$, for all $\mathbf{m} \in Z^n$. Eq. (3.3) shows that sampling of the function f_1 replaces its Fourier transform $\hat{f}_1$ by a superposition of shifted copies of $\hat{f}_1$.

Suppose the spectrum of the original function f is contained in an open sphere $P = \{\mathbf{k} \in R^n \mid \|\mathbf{k}\| < R\}$ of radius R, i.e., $\hat{f}(\mathbf{k}) = 0$ if $\mathbf{k} \notin P$. Because of Lemma 1 this implies that $\hat{f}_1(\mu) = 0$ if $\mu \notin V^{\mathrm{T}}P = Q$. Thus the spectrum of f_1 is contained in a region Q, which is the skewed image of a sphere. Define

$$\begin{aligned} Q_l &= l + Q = \{l + \mu \mid \mu \in Q\}, \\ P_l &= UQ_l, \end{aligned} \tag{3.4}$$

for all $l \in Z^n$.

In order to be able to recover the sampled function, the regions Q_l should be mutually disjunct, $Q_l \cap Q_{\mathbf{m}} = \varnothing$ if $l \neq \mathbf{m}$, as follows. If the Q_l's are disjunct, the sum of Eq. (3.3) reduces to at most one term:

$$\hat{g}_1(\mu) = \begin{cases} \hat{f}_1(\mu - l) & \text{if } \mu \in Q_l \\ 0 & \text{if } \mu \notin Q_l, \text{ all } l. \end{cases} \tag{3.5}$$

This implies that the values of $\hat{g}_1$ on the unit cell $D = \{\mu \mid 0 \leqslant \mu_i < 1, \text{ all } i\}$ contain all information needed to calculate $\hat{f}_1$. (*Proof.* Let $\mu \in R^n$. If $\mu \notin Q$ then $\hat{f}_1(\mu) = 0$. If $\mu \in Q = Q_0$ then $\hat{f}_1(\mu) = \hat{g}_1(\mu)$. Let $\mu_i = m_i + \alpha_i$, $0 \leqslant \alpha_i < 1$, so that $\mu = \mathbf{m} + \alpha$, and $\alpha \in D$. Because $\hat{g}_1$ is periodic, $\hat{g}_1(\mu) = \hat{g}_1(\alpha)$, and this value is known. Q.E.D.)

Thus sampling does not result in any loss of information, and $\hat{f}_1$, and hence f_1 and f can be fully reconstructed from the values of $\hat{g}_1$ on D. If the Q_l's are not disjunct, this is not possible. See Fig. 1 for an illustration of a set of disjunct Q_l's.

The Q_l's are disjunct, if and only if the P_l's are disjunct, because U is invertible. But $P_l = U(l+Q) = Ul + P$ is a sphere of radius R with center $Ul = U(\sum_{j=1}^{n} l_j \mathbf{e}_j) = \sum_{j=1}^{n} l_j \mathbf{u}_j$. Thus the centers of the spheres P_l form a lattice defined by the vectors $\mathbf{u}_j$. These spheres are shown by Fig. 2.

As a result of the above, it can be said that the function f is *adequately* sampled if the spheres P_l are packed in a lattice, without overlapping. On the other hand, the function f is *efficiently* sampled if the spheres are packed as dense as possible. This

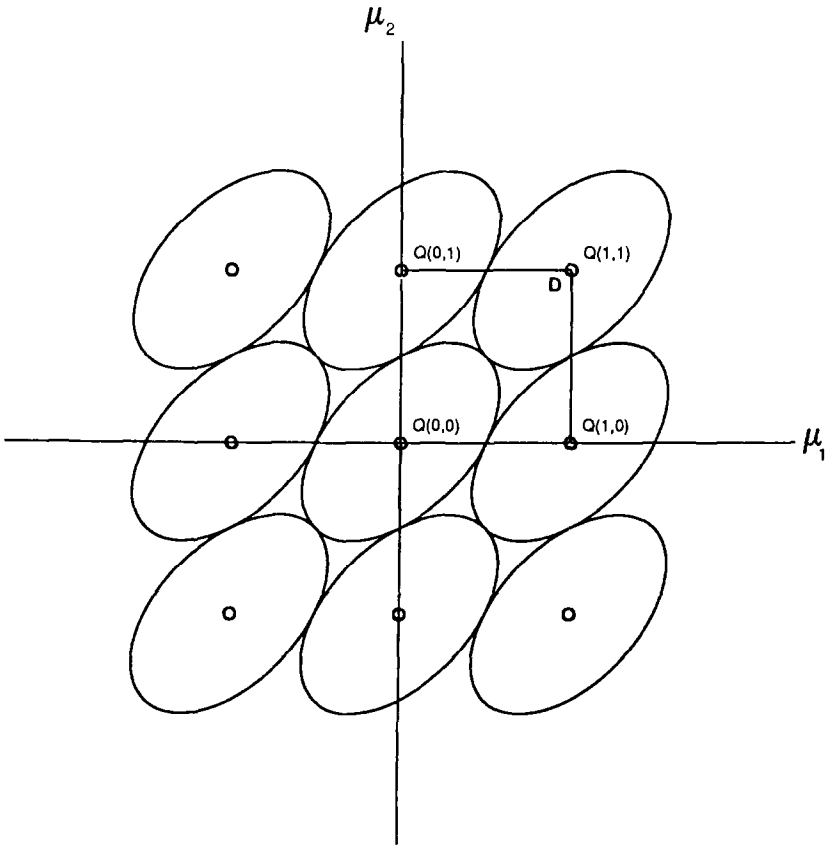

FIG. 1. The $\boldsymbol{\mu}$-spectrum of a function f sampled on a two-dimensional skewed grid. The Fourier transform of f is contained in a sphere P_0, so that the Fourier transform of the function in the oblique coordinates, $\hat{f}_1(\boldsymbol{\mu})$, is contained in the egg-shaped region Q_0. Sampling the function f on a discrete grid produces copies of $\hat{f}_1(\boldsymbol{\mu})$, each contained in an egg-shaped region Q_l. Since the regions $Q_l = l + Q_0$ are disjunct, these copies do not overlap each other, so that no aliasing occurs. (*Aliasing* is the phenomenon of one frequency impersonating another; this effect is caused by undersampling). The lattice vectors that define the sampling grid are $\mathbf{v}_1 = \binom{2/\sqrt{3}}{0}$, and $\mathbf{v}_2 = \binom{1/\sqrt{3}}{1}$. The band-limit radius is $R = 0.5$.

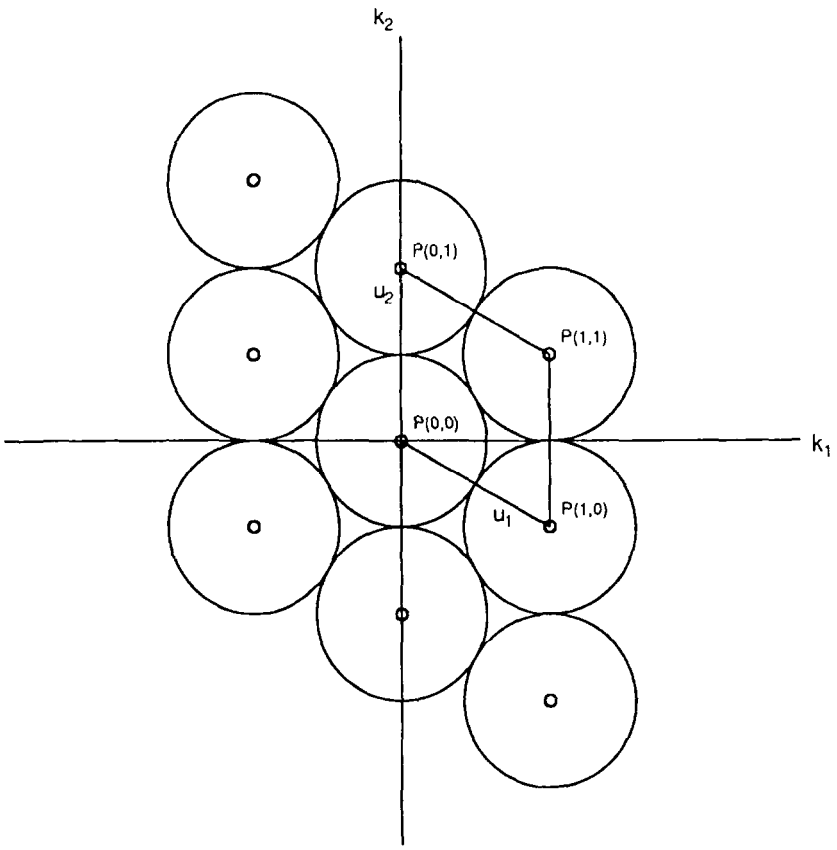

FIG. 2. The **k**-spectrum of a function f sampled on a two-dimensional skewed grid. The Fourier transform of f is contained in the sphere P_0. Sampling the function f on a discrete grid produces copies of $\hat{f}(\mathbf{k})$, each contained in a sphere with radius R and center Ul. Since the regions $P_l = Ul + P_0$ are disjunct, these copies do not overlap each other, so that no aliasing occurs. The lattice vectors that define the sampling grid are the same as in Fig. 1. The reciprocal lattice vectors that define the lattice in **k**-space are $\mathbf{u}_1 = \begin{pmatrix} 3/2 \\ -1/2 \end{pmatrix}$, and $\mathbf{u}_2 = \begin{pmatrix} 0 \\ 1 \end{pmatrix}$. The band-limit radius is $R = 0.5$. The spheres fill 90.7% of all space. (Sampling by a rectangular grid only fills 78.5% of all space.)

can be seen by the following argument: Let η be the part of **k**-space that is occupied by spheres P_l,

$$\eta = \frac{\text{Vol(spheres)}}{\text{Vol(space)}} = \frac{\text{Vol(one sphere)}}{\text{Vol(one unit cell)}}, \tag{3.6}$$

since the number of unit cells equals the number of spheres. The volume of the unit cell is $|\det U| = d$. If for a given radius R the unit cell is made as small as possible, then $|\det V| = 1/d$, the volume of a unit cell in **x**-space, is made as large as possible. Since the number of unit cells in **x**-space equals the number of sampling points, this

TABLE I

Isotropic Sampling Efficiency[a]

Dimension	Maximum sampling efficiency η_{max} (%)	Efficiency of cubic lattice η_{cub} (%)	Improvement factor η_{max}/η_{cub}
1	100.0	100.0	1.0
2	90.7	78.5	1.15
3	74.0	52.4	1.4
4	61.7	30.8	2.0
5	46.5	16.45	2.8
6	37.3	8.07	4.6
7	29.5	3.69	8.0
8	8.07	0.505	16.0

[a] Source: Petersen and Middleton [6].

minimizes the number of sampling points needed to sample a certain volume of space adequately with isotropic band-limit R. Thus η may be termed the *isotropic sampling efficiency*.

The problem of finding the densest possible lattice packing of spheres has been solved [2], for dimensions at least up to $n = 8$. Table I, which is adapted from Table C.II of Ref. [6], shows the maximum obtainable efficiency η_{max}, the efficiency η_{cub} obtained by using a cubic lattice, and the improvement achievable by skewed sampling. It can easily be shown that η_{cub} equals the volume of a sphere of radius $R = \frac{1}{2}$ in n-dimensional space, and that the improvement factor η_{max}/η_{cub} equals $|\det V|$, where V is the matrix that defines the sampling grid in the **x**-domain.

From the table, it is evident that in multi-dimensions sampling by a cubic lattice is much less efficient than sampling by an appropriately skewed lattice. This implies that the standard Fourier method is also much less efficient than the skewed Fourier method.

Optimal sampling grids for $n \leqslant 8$ are presented in Table II, which is adapted from Table C.I of Ref. [6]. The table gives for each dimension the matrix V which defines an optimal sampling lattice in **x**-space. The spheres packed in **k**-space are of radius $R = \frac{1}{2}$. For other radii R all the elements of the matrix V should be divided by $2R$. The optimal lattice is not unique, since rotation of the given lattice produces other optimal lattices. The lattice given in the table should thus be rescaled, rotated, and translated to fit the particular problem to be solved.

IV. The Skewed Fourier Algorithm

The results obtained in the previous section for sampling of f are equally valid for sampling of $\nabla^2 f$, since f and $\nabla^2 f$ have the same band-limit radius R (cf.

TABLE II

Optimal Sampling Lattices, for Dimension Up to $n = 8$

$n = 1, 2, 3, 4, 5$: $V = (1)$,

$$\begin{bmatrix} \frac{2}{\sqrt{3}} & \frac{1}{\sqrt{3}} \\ 0 & 1 \end{bmatrix}, \quad \begin{bmatrix} \frac{1}{\sqrt{2}} & 0 & \frac{1}{\sqrt{2}} \\ \frac{1}{\sqrt{2}} & 0 & \frac{-1}{\sqrt{2}} \\ \frac{1}{\sqrt{2}} & \sqrt{2} & \frac{1}{\sqrt{2}} \end{bmatrix}, \quad \begin{bmatrix} 1 & 0 & 0 & 0 \\ 1 & 2 & 1 & 1 \\ 0 & 0 & 1 & 0 \\ 0 & 0 & 0 & 1 \end{bmatrix}, \quad \begin{bmatrix} 1 & 0 & 0 & 0 & 0 \\ 0 & 0 & \sqrt{2} & \frac{1}{\sqrt{2}} & \frac{1}{\sqrt{2}} \\ 1 & 2 & 2 & 1 & 1 \\ 0 & 0 & 0 & 1 & 0 \\ 0 & 0 & 0 & 0 & 1 \end{bmatrix}$$

$n = 6, 7$: $V =$

$$\begin{bmatrix} 1 & 0 & 0 & 0 & 0 & 0 \\ 0 & 0 & \sqrt{2} & \frac{1}{\sqrt{2}} & 0 & \frac{1}{\sqrt{2}} \\ 1 & 2 & 2 & 1 & 0 & 1 \\ \frac{\sqrt{2}}{\sqrt{3}} & \frac{2\sqrt{2}}{\sqrt{3}} & \sqrt{6} & \frac{5}{\sqrt{6}} & \frac{2\sqrt{2}}{\sqrt{3}} & \frac{\sqrt{3}}{\sqrt{2}} \\ 0 & 0 & 0 & 1 & 0 & 0 \\ 0 & 0 & 0 & 0 & 0 & 1 \end{bmatrix}, \quad \begin{bmatrix} 1 & 0 & 0 & 0 & 0 & 0 & 0 \\ 0 & 0 & 1 & 0 & 0 & 0 & 0 \\ \frac{1}{\sqrt{2}} & \sqrt{2} & \frac{1}{\sqrt{2}} & 0 & 0 & 0 & 0 \\ \frac{1}{\sqrt{6}} & \frac{\sqrt{2}}{\sqrt{3}} & \frac{\sqrt{3}}{\sqrt{2}} & \frac{2\sqrt{2}}{\sqrt{3}} & 0 & 0 & \frac{\sqrt{2}}{\sqrt{3}} \\ \frac{2}{\sqrt{3}} & \frac{4}{\sqrt{3}} & 2\sqrt{3} & \frac{8}{\sqrt{3}} & 2\sqrt{3} & \sqrt{3} & \frac{4}{\sqrt{3}} \\ 0 & 0 & 0 & 0 & 0 & 1 & 0 \\ 0 & 0 & 0 & 0 & 0 & 0 & 1 \end{bmatrix}$$

$n = 8$: $V =$

$$\begin{bmatrix} 1 & 0 & 0 & 0 & 0 & 0 & 0 & 0 \\ 0 & 0 & 1 & 0 & 0 & 0 & 0 & 0 \\ \frac{1}{\sqrt{2}} & \sqrt{2} & \frac{1}{\sqrt{2}} & 0 & 0 & 0 & 0 & 0 \\ \frac{1}{\sqrt{10}} & \frac{\sqrt{2}}{\sqrt{5}} & \frac{3}{\sqrt{10}} & \frac{2\sqrt{2}}{\sqrt{5}} & 0 & 0 & 0 & 0 \\ \frac{2}{\sqrt{35}} & \frac{4}{\sqrt{35}} & \frac{6}{\sqrt{35}} & \frac{8}{\sqrt{35}} & \frac{2\sqrt{5}}{\sqrt{7}} & 0 & 0 & \frac{\sqrt{5}}{\sqrt{7}} \\ \frac{4}{\sqrt{7}} & \frac{8}{\sqrt{7}} & \frac{12}{\sqrt{7}} & \frac{16}{\sqrt{7}} & \frac{20}{\sqrt{7}} & 2\sqrt{7} & \sqrt{7} & \frac{10}{\sqrt{7}} \\ 0 & 0 & 0 & 0 & 0 & 0 & 1 & 0 \\ 0 & 0 & 0 & 0 & 0 & 0 & 0 & 1 \end{bmatrix}$$

Note. This table presents the matrices V, whose column vectors $\mathbf{v}_j$ define the sampling lattice. The matrices V are normalized, so that the band-limit radius is $R = \frac{1}{2}$. The matrices U, whose column vectors define a dense lattice packing of spheres can be obtained by $U = (V^{-1})^{\mathrm{T}}$. Adapted and corrected from: Petersen and Middleton [6].

Eq. (2.27)). In particular, the Fourier transform of the Laplacian, $L(\boldsymbol{\mu})\,\hat{f}_1(\boldsymbol{\mu})$, is replicated at all the lattice points, as a result of the sampling procedure.

Let G be the function which replicates $L|_Q$ (the restriction of L to Q), i.e.,

$$G(\boldsymbol{\mu}) = \begin{cases} L(\boldsymbol{\mu} - \boldsymbol{l}) & \text{if } \boldsymbol{\mu} \in Q_{\boldsymbol{l}} \\ 0 & \text{if } \boldsymbol{\mu} \notin Q_{\boldsymbol{l}}, \text{ all } \boldsymbol{l}, \end{cases} \tag{4.1}$$

in analogy with Eq. (3.5). It is easy to see that the function $G(\boldsymbol{\mu})\,\hat{g}_1(\boldsymbol{\mu})$ is the Fourier transform of the sampled Laplacian, and that it is a periodic function. All information on G is thus contained in the set of values of G on the unit cell D. As a result, computing the sampled Laplacian amounts to performing a Fourier transform, multiplying by G, and performing an inverse Fourier transform.

The procedure outlined above can be implemented by the following algorithm:

ALGORITHM FOR COMPUTATION OF THE LAPLACIAN.

(S1) Discretize the function f on a finite grid, by representing its values at grid points $\mathbf{x} = (1/2R) \sum_{j=1}^{n} m_j \mathbf{v}_j$, where $\mathbf{m} = (m_1, ..., m_n)$ is a multi-index number, and $0 \leqslant m_j \leqslant N_j - 1$. R is the desired band-limit radius. The $\mathbf{v}_j$ are the column vectors of the transformation matrix obtained from Table II.

(S2) Compute the n-dimensional discrete Fourier transform by the fast Fourier transform algorithm, with M_j points in direction j.

(S3) Compute the value $G(\boldsymbol{\mu})$ for each grid point indexed $\mathbf{m}$, as follows: Let $\boldsymbol{\mu} = (m_1/N_1, ..., m_n/N_n)$ and $\mathbf{k} = U\boldsymbol{\mu}$. Find the sphere $P_{\boldsymbol{l}}$ of radius R to which $\mathbf{k}$ belongs, by computing the distance $\|\mathbf{k} - U\boldsymbol{l}\|$ of $\mathbf{k}$ to all corners $U\boldsymbol{l}$ of the unit cell, where $\boldsymbol{l} = (l_1, ..., l_n)$ with $l_j \in \{0, 1\}$. If $\mathbf{k} \in P_{\boldsymbol{l}}$, then compute $G(\boldsymbol{\mu}) = -4\pi^2 \sum_{k=1}^{n} \sum_{j=1}^{k} c_{jk}(\mu_j - l_j)(\mu_k - l_k)$. If no such $P_{\boldsymbol{l}}$ exists, then set $G(\boldsymbol{\mu}) = 0$.

(S4) Multiply the function value at the grid point $\mathbf{m}$ by $G(\boldsymbol{\mu})$.

(S5) Perform an inverse fast Fourier transform.

(S6) Retrieve the values of $\nabla^2 f$ from the grid in the same discretization as in step (S1).

Some remarks on the algorithm:

(i) Step (S3), the preparation of the quadratic form, has to be performed only once, for computation of many Laplacians on the same grid. The values $G(\boldsymbol{\mu})$ can be stored on a separate grid, and used in subsequent computations of Laplacians.

(ii) For functions f that are band-limited only in approximation, step (S3) implies a cutoff of the spectrum at radius R. An alternative to this is the assignment of a value $G(\boldsymbol{\mu})$ *in any case*, according to the nearest corner. In Section V it is shown that this improves accuracy in the test case of a Gaussian wave function.

The skewed Fourier method solves the time dependent Schrödinger equation by

the same algorithm as the Fourier method (see [8–9]), except for the computation of the Laplacian, which is done by the algorithm presented above.

V. Numerical Test: Five-Dimensional Gaussian Wave Functions

Two Gaussian wave functions were used to compare the accuracy of the Laplacian operator on orthogonal and skewed grids. Gaussian functions were chosen because such functions approximate extremely well a band-limited function with a finite support. Moreover, they resemble closely semi-local wave functions which are commonly used in molecular dynamics.

Figure 3 shows the position of the Gaussians in momentum space relative to the outer boundaries of the band-limiting radius, for both grid geometries. This is visualized by a two-dimensional cut through the five-dimensional momentum space, where the Gaussians are characterized by their average momentum $\mathbf{p}_0$ and their width Δp. The momentum of one Gaussian was directed along an axis of the orthogonal grid; the other Gaussian was directed diagonally. The infinite spread in momentum of the Gaussians means that part of the function always penetrates into

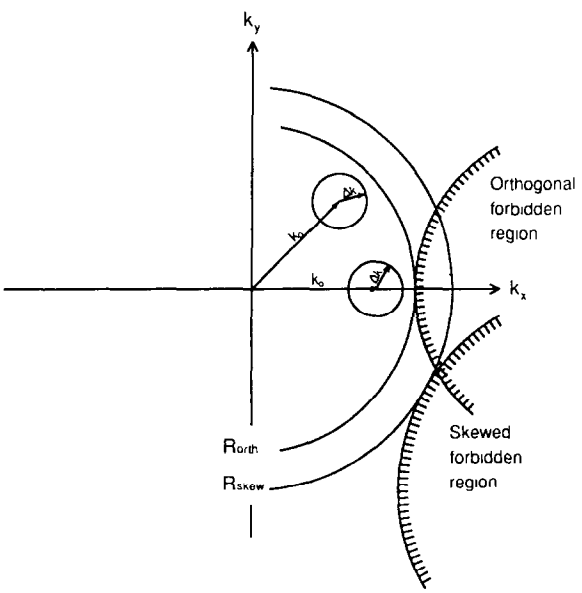

Fig. 3. The momentum and momentum spread of two five-dimensional Gaussian wave functions, relative to the band-limits of the orthogonal and skewed grid. Shown is the intersection through the k_x, k_y plane. The length of the mean momentum vector $\|\mathbf{k}_0\| = 0.5$ The radius of the circles is one standard deviation, which means that in five dimensions 13% of the Gaussian function is inside the ball of this radius. R_{orth} is the band-limiting radius of the orthogonal grid; R_{skew} is the band-limiting radius of the skewed grid. The intersection of one of the forbidden balls with the k_x, k_y plane is also displayed. The forbidden region represents aliasing.

TABLE III

Accuracy of the Skewed Fourier Laplacian

Number of points in each direction N_i	Volume of sampling unit cell $\lvert\det V\rvert$	Band-limit radius R		Wave number vector $\mathbf{k}_0^T$	Accuracy (with band-limit cutoff)		Accuracy (without cutoff)	
		Skewed	Orthogonal		Skewed	Orthogonal	Skewed	Orthogonal
15	0.2441	0.816	0.663	(0.5, 0, 0, 0, 0)	0.13	0.41	0.012	0.093
				$(1, 1, 1, 1, 1)/2\sqrt{5}$	0.14	0.49	0.0095	0.0054
18	0.0981	0.979	0.795	(0.5, 0, 0, 0, 0)	0.014	0.16	0.00054	0.014
				$(1, 1, 1, 1, 1)/2\sqrt{5}$	0.017	0.18	0.0017	0.00018

Note The computation is tested for a five-dimensional Gaussian wave function $f(\mathbf{x}) = e^{2\pi i \mathbf{k}_0 \cdot \mathbf{x}} e^{-\mathbf{x} \cdot \mathbf{x}/2}$. The Gaussian has momentum $\mathbf{p}_0 = 2\pi\mathbf{k}_0$. The skewed sampling is the optimal sampling, as given by Table II. Results are compared with results of the Fourier method on an orthogonal grid, for the same volume of the sampling unit cell. The radius R is the band-limit radius $R = |\mathbf{k}_{\max}|$, the maximum wave number for which the sampling is adequate.

the forbidden regions, see Fig. 3. The axially directed function is the worst case for the orthogonal grid. This can be seen by the large relative error given in Table III for this case. For the skewed grid the forbidden regions are further out, and therefore the tails of the momentum penetrate much less into the regions; this explains the smaller maximum error obtained for the skewed grid, as compared to the error on the orthogonal grid (for the same density of grid points), see Table III. It should be noticed in both cases that the procedure without a band-limit cutoff (the alternative procedure for step (S3)) always gave superior results.

A priori the direction of the wave function is not known, therefore the error analysis should consider the worst case. Table III shows that the accuracy of the worst case of the skewed grid with 15^5 points is better than the accuracy of the worst case of the orthogonal grid with 18^5 points. The numerical effort is approximately proportional to the total number of grid points; the ratio between the two cases is 2.49, which confirms the theoretical prediction that the skewed grid is 2.8 times more efficient in sampling (see Table I).

VI. Example: Two Interacting Triplet Hydrogen Atoms in a Box

Hydrogen atoms can be prevented from recombining by placing them in a magnetic field [10]. As an illustration of the skewed Fourier method the ground and first excited states of two interacting triplet hydrogen atoms are calculated as a function of the volume of the box that contains them. Out of this calculation the deviation of hydrogen atomic gas from ideal gas behavior for low temperatures is obtained directly.

The Hamiltonian of the system is given by

$$\hat{\mathbf{H}} = -\frac{\nabla_1^2}{2m} + \mathbf{V}(\mathbf{r}_1) - \frac{\nabla_2^2}{2m} + \mathbf{V}(\mathbf{r}_2) + \mathbf{V}_{12}(r_{12}), \tag{6.1}$$

where $\mathbf{r}_i$ is the position vector of atom $i = 1, 2$, and r_{12} is the relative distance between them. The interaction potential is adopted from the work of Tang and Toennies [11]. $\mathbf{V}(\mathbf{r}_i)$ is the potential due to the magnetic field. The eigenstates and eigenvalues of this system are calculated by a relaxation scheme in which an initial guess of the eigenfunction is propagated in imaginary time. The ground state is the only state that eventually survives. The propagation is done by a Chebychev expansion of the evolution operator $U(\tau) = \exp(-\hat{\mathbf{H}}\tau)$. The first excited state is calculated

TABLE IV

Parameters of Potential, Grid, and Propagation Method, Used in the Calculation of the Eigenfunctions of Two Interacting Triplet Hydrogen Atoms

Potential Parameters			
Interaction potential	K. T Tang and J. P. Toennies	Ref. [11]	
	Repulsive part	$A \exp(-br_{12})$	
		$A = 9.30$	
		$b = 1.664$	
	Attractive part	$-\sum_{n\geq 3}\left[1-\sum_{k=0}^{2n}\frac{(br_{12})^k}{k!}\exp(-br_{12})\right]\frac{C_{2n}}{r_{12}^{2n}}$	
		$C_6 = 6.499$	
		$C_8 = 124\,4$	
		$C_{10} = 3.286 \times 10^3$	
		$C_{12} = 1\,215 \times 10^5$	
		$C_{14} = 6\,061 \times 10^6$	
		$C_{16} = 3.938 \times 10^8$	
	Minimum energy	$\varepsilon = -2\,05 \times 10^{-5}$	
	Equilibrium distance	$R_m = 7\,80$	
Box potential		$\mathbf{V}(\mathbf{r}_i) = 0$	
Grid Parameters			
$N = N_1 = N_2 = N_3 = N_4 = N_5 = N_6$			
Number of grid points N	4	6	8
Total number of points	4096	46656	262144
Minimum grid spacing $\Delta x_{\min}$	1.5	1	0.75
Maximum density	9.259×10^{21} molecules/cm^3		
Maximum grid spacing $\Delta x_{\max}$	3	2.	1.5
Minimum density	1.157×10^{21} molecules/cm^3		
Chebychev Time Propagation			
Propagation time	$t = 60000$		
Number of Hamiltonian Calculations	$M = 200$	(for $\Delta x = 1$)	
Mass	$m = 1823$		

Note. All parameters are in atomic units.

by projecting the ground state out of the Hilbert space. The details of the method can be found elsewhere [12]. The initial wavefunction is chosen as a symmetric combination of the wavefunctions of the two hydrogen atoms. Because the Hamiltonian does not mix the symmetry the propagated eigenstates conserve the correct symmetry. For long propagation times random errors can destroy the symmetry. This difficulty is overcome by a symmetrization procedure which is carried out to restore the correct symmetry. The optimal oblique six-dimensional grid was chosen for the calculation. Table IV summarizes the potential and grid parameters used for the calculation. Figure 4 shows the ground state energy as a function of the box volume of the two interacting hydrogen atoms. The convergence is checked by increasing the number of grid points from $4^6 = 4096$ to $6^6 = 46656$ to $8^6 = 262144$ points. For a box of volume $V = 8^3 = 256au$, the ground state energy changed from 1.701×10^{-5} for the coarse grid to 1.383×10^{-5} for the intermediate grid and 1.211×10^{-5} for the fine grid. Figure 5 displays the excited state energy compared with the energy of two non-interacting hydrogen atoms in a box. Examining Figs. 4

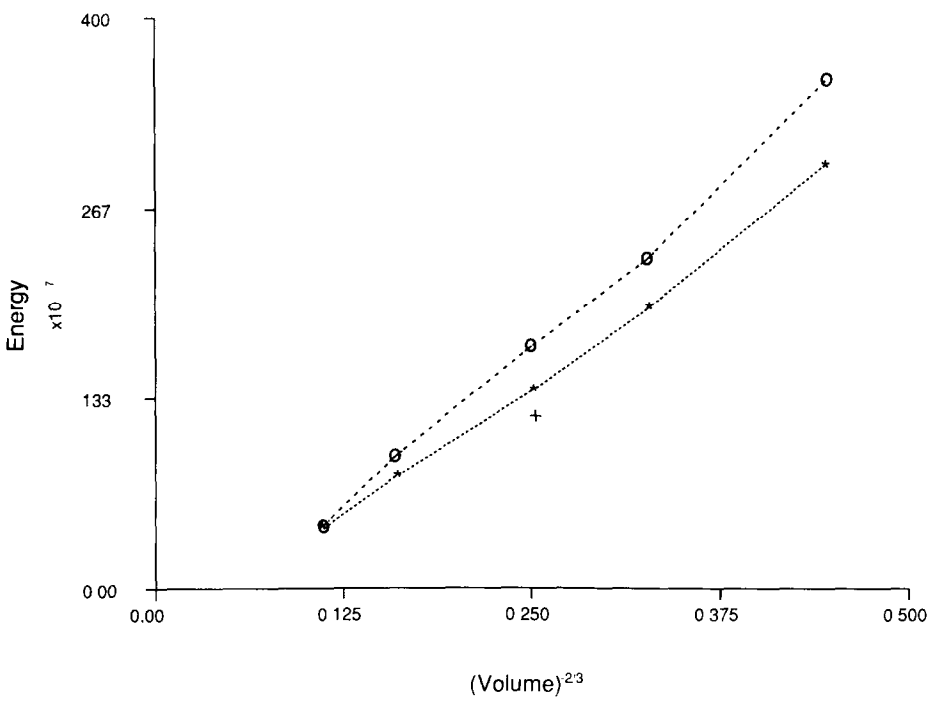

FIG. 4. The energy of the ground state as a function of $(\text{volume})^{-2/3}$ of the box containing two interacting triplet hydrogen atoms. The convergence of the method is displayed. The dashed-dotted line (–·–) is the result of the calculation using 4^6 grid points. The calculated values are marked by (∘). The dashed line (– – –) is the result of the 6^6 grid point calculation. The calculated values are marked by (*). The (+) sign is the result of the 8^6 grid point calculation, which was performed for only one energy value. The units are atomic units.

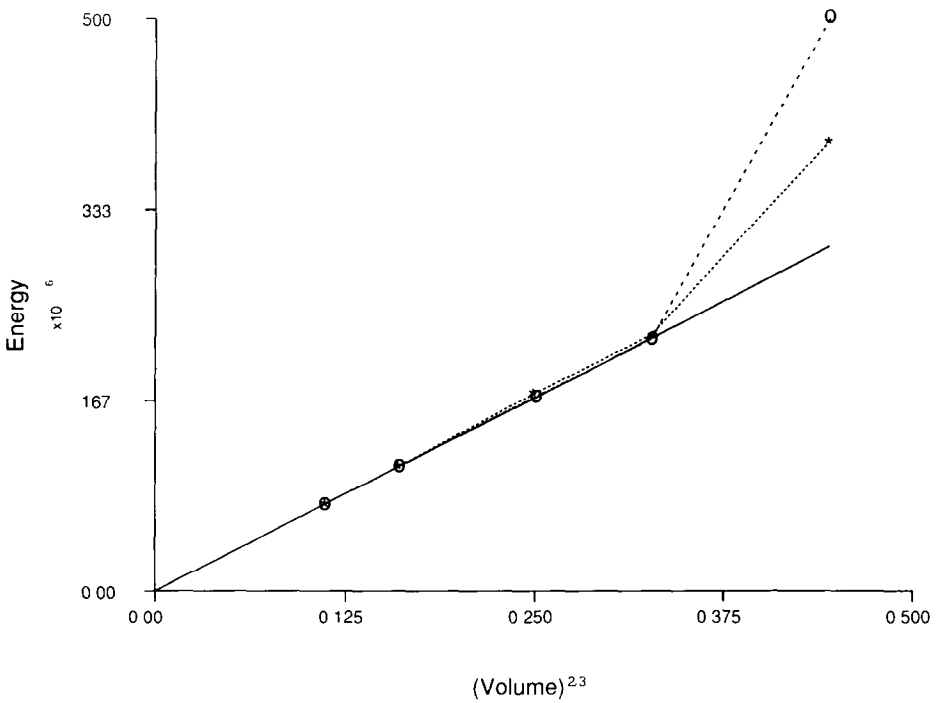

FIG. 5. The energy of the first excited state of the two interacting atoms as compared to the energy of the excited state without interaction plotted as a function of $(\text{volume})^{-2/3}$. The dashed-dotted line $(-\cdot-)$ is the result of the 4^6 point calculation; the dashed line is the result of the 6^6 point calculation; and the solid line is the reference energy of two particles in a box without interaction.

and 5 one finds, as expected, that for boxes of large volume, using the coarse grid is sufficient for convergence. When the hydrogens are condensed together a finer grid is required to sample the interaction potential correctly.

A calculation of one energy value on the coarse grid of 4096 points took 3 min on a CCI Power 32 minicomputer with 16 MB of internal memory. The same energy calculation took 120 min for a grid of 46656 points and 1200 min for the fine grid of 262144 points.

VII. DISCUSSION

Use of the skewed Fourier method instead of the standard Fourier method becomes already attractive at dimensions $n \gtrsim 3$ and imperative at dimensions $n \gtrsim 5$, since high-dimensional problems are very demanding in terms of computational resources. For example, in Section V the number of points for calculation of the five-dimensional Laplacian was reduced from $18^5 = 1889568$ points to $15^5 = 759375$

points. This may mean the difference between a feasible and an unfeasible calculation. In the calculation of Section VI the number of points would have increased from 262144 in the skewed Fourier method to approximately 1,200,000 for the Cartesian Fourier method. Such a calculation would be unfeasible on the CCI minicomputer.

CPU-time scaling laws are important guidelines when considering the feasibility of a calculation. The CPU-time needed for wave propagation by the Fourier method is the product of the CPU-time needed for a single Hamiltonian operation and the number of such operations needed to complete the propagation.

The cost of a Hamiltonian operation is mainly determined by the CPU-time of the forward and backward FFTs, which scales semilinearly with the total number of grid points N as $O(N \log N)$. The number N is proportional to the volume of the coordinate momentum phase-space volume $= (2p_{\max} \cdot l)^n$, where l is the extent of the grid, $p_{\max}$ the cutoff in momentum and n the dimensionality of the problem. The smallest number of points needed to approximate this phase-space is: $N = \text{volume}/h$.

The number M of Hamiltonian operations needed is proportional to the volume of the time-energy phase-space, $M \approx \Delta E \cdot t$, where ΔE is the range of energy eigenvalues represented on the grid, and t is the propagation time. This scaling law is valid for both the second order finite-differencing [8] and the Chebychev propagation scheme [9].

The total CPU-time needed according to the considerations above is $O(E^{n/2} \log E) = O(p_{\max}^{n+2} \log p_{\max})$ provided that the kinetic energy dominates the calculation. For parallel computing devices these scaling estimates may change.

A necessary condition for the use of the Fourier pseudospectral method is an ordered, evenly sampled grid. The representation of the wave function by an ordered grid can never be completely isotropic, therefore some waste is unavoidable. Geometrically, this can be understood by the fact that there is always empty space between multi-dimensional packed spheres. This empty space increases with dimensionality; for example in eight dimensions 92% of the space is wasted, see Table I. On this basis one can speculate that the Fourier pseudospectral method will become too wasteful for dimensions larger than 10. This conclusion must be restricted, because it is not understood what effect the filling procedure of the empty space has on the accuracy of the method.

An important issue in the use of the skewed Fourier method should be briefly mentioned. All Fourier pseudospectral methods require periodic boundary conditions. In the skewed Fourier method this fact can be used to repack the grid points to construct any kind of parallelepiped, such as a rectangular box.

Realistic multi-dimensional problems of weakly interacting gasses such as helium or triplet hydrogen can be treated using this method on existing computers today. The real computational challenge of chemistry, the six-dimensional reactive scattering A + BC is beyond the scope of existing computers. However, the development of more powerful hardware will bring such problems within reach in the near future. Use of the skewed Fourier method might then make problems solvable that the standard Fourier method would not be able to handle.

ACKNOWLEDGMENTS

We thank Professor M. Cohen for his encouragement and helpful suggestions. Work was supported by the United States Israel Binational Foundation. The Fritz Haber Research Center is supported by the Minerva Gesellschaft für die Forschung, GmbH München, BRD.

REFERENCES

1. D. GOTTLIEB AND S. A. ORZAG, "Numerical Analysis of Spectral Methods: Theory and Applications" (SIAM, Philadelphia, 1977); D. GOTTLIEB, M. Y. HUSSAINI, AND S. A. ORSZAG, *in* "Spectral Methods for Partial Differential Equations," edited by R. G. Voigt, D. Gottlieb and M. Y. Hussaini, (SIAM, Philadephia, 1984), p. 1.
2. H. S. M. COXETER, *Canad. J. Math.* **3**, 391 (1951).
3. C. A. ROGERS, "Packing and Covering" (Cambridge Univ. Press, Cambridge, 1964).
4. J. H. CONWAY AND N. J. A. SLOANE, "The Leech Lattice, Sphere Packings, and Related Topics" (Springer-Verlag, Berlin, 1984).
5. N. J. A. SLOANE, *IEEE Trans. Inform. Theory* **27**, 327 (1981).
6. D. P. PETERSEN AND D. MIDDLETON, *Inform. and Control* **5**, 279 (1962).
7. R. N. BRACEWELL, "The Fourier Transform and its Applications," 2nd ed. (McGraw-Hill, New York, 1978).
8. D. KOSLOFF AND R. KOSLOFF, *J. Comput. Phys.* **52**, 35 (1983).
9. H. TAL-EZER AND R. KOSLOFF, *J. Chem. Phys.* **81**, 3967 (1984).
10. I. F. SILVERA AND J. T. M. WALRAVEN, *Phys. Rev. Lett.* **44**, 164 (1980); J. T. M. WALRAVEN, I. F. SILVERA, AND A. P. M. MATTHEY, *Phys. Rev. Lett.* **45**, 449 (1980); YU. KAGAN AND G. V. SHLYAPNIKOV, *Phys. Lett. A* **95**, 309 (1983).
11. K. T. TANG AND J. P. TOENNIES, *J. Chem. Phys.* **80**, 3726 (1984).
12. R. KOSLOFF AND H. TAL-EZER, *Chem. Phys. Lett.* **127**, 223 (1986).